FOSSIL ENERGY

DOE/BC/15211-20
(OSTI ID: 795239)

AN EFFECTIVE CONTINUUM MODEL FOR THE GAS EVOLUTION IN INTERNAL STEAM DRIVES

Topical Report
January 2002

By
Ioannis N. Tsimpanogiannis
Yanis C. Yortsos

Date Published: June 2002

Work Performed Under Contract No. DE-AC26-99BC15211

University of Southern California
Los Angeles, California

National Energy Technology Laboratory
National Petroleum Technology Office
U.S. DEPARTMENT OF ENERGY
Tulsa, Oklahoma

DOE/BC/15211-20
Distribution Category UC-122

An Effective Continuum Model for the Gas Evolution in Internal Steam Drives

By
Ioannis N. Tsimpanogiannis
Yanis C. Yortsos

June 2002

Work Performed Under DE-AC26-99BC15211

Prepared for
U.S. Department of Energy
Assistant Secretary for Fossil Energy

Jerry Casteel, Project Manager
National Petroleum Technology Office
P.O. Box 3628
Tulsa, OK 74101

Prepared by
Department of Chemical Engineering
University of Southern California
University Park Campus
HEDCO 316, USC
Los Angeles, CA 90089-1211

Table of Contents

ABSTRACT

We derive an effective continuum model to describe the nucleation and subsequent growth of a gas phase from a supersaturated liquid in a porous medium, driven by heat transfer. The evolution of the gas results from the reduction of the system pressure at a constant rate. The model addresses two stages before the onset of bulk gas flow, nucleation and gas phase growth. The problem arises in internal steam drives, for example of the type recently discussed in blowdown experiments in carbonate rocks (Dehghani et al., 1997, Dehghani and Kamath, 1999).

Important quantities characterizing the process, such as the fraction of pores that host activated sites, the deviation from thermodynamic equilibrium, the maximum supersaturation in the system and the critical gas saturation depend crucially on the nucleation characteristics of the medium. We use heterogeneous nucleation models in the form of pre-existing gas, trapped in hydrophobic cavities to investigate the nucleation behavior. Using scaling analysis and a simpler analytical model we show that the relevant quantities during nucleation can be expressed in terms of a simple combination of dimensionless parameters, which include rate effects. The subsequent evolution of the gas phase and the approach to the critical gas saturation are also described using numerical and analytical models.

The theory predicts that the maximum supersaturation in the system is a weakly increasing function of the decline rate. This function depends sensitively on the probability density function of the nucleation cavity sizes. It also predicts that the final nucleation fraction, thus the critical gas saturation, is a power law of the decline rate. The theory for both nucleation and phase growth is then compared with available experimental data and a good match is obtained by appropriate fitting of the nucleation characteristics of the medium.

I. INTRODUCTION

The liquid-to-gas phase change in a porous medium and the subsequent growth of the gas phase is encountered in a plethora of applications driven by mass or heat transfer. Typical examples include the solution gas-drive process for the recovery of oil from oil reservoirs, boiling in porous media, thermal methods for oil recovery, nuclear waste disposal, soil remediation and others. In this report, we examine the gas phase growth from a supersaturated, slightly compressible, liquid in a porous medium, driven by heat transfer and controlled by the application of a constant-rate decline of the system pressure. A characteristic example of such a process occurs dyring cyclic steaming for the recovery of oil from low permeability reservoirs through hydraulic or natural fractures (Dehghani et al., 1997). During injection and soaking, steam condenses in the fracture and hot water imbibes into the matrix. During production, the pressure of the system constantly declines, and when it falls sufficiently below the vapor pressure, it results in the appearence of steam in the matrix (in-situ boiling). The in-situ production and subsequent growth of the steam phase inside the matrix are of interest because they result in expelling additional oil from the matrix.

Dehghani et al. (1997) conducted a series of core experiments in order to study the effect of in-situ steam drive on fluid displacement in porous media. Subsequently, Dehghani and Kamath (1999) conducted experiments with a vuggy carbonate core using a recombined oil to study the contribution of the various recovery mechanisms (thermal expansion, thermally enhanced solution gas drive, dry distillation, and in-situ steam drive) during steam injection, followed by pressure reduction.

While of interest both from theoretical and applied viewpoints, a more fundamental understanding of the basic aspects of this process has not been obtained, to our knowledge. It is the objective of this report to bridge this gap, by providing a model both of the nucleation and of the gas-phase growth periods. Internal steam drive has many similarities with the process of solution gas-drive. They both describe the evolution of a gas phase due to the increase of the supersaturation of the system, through a relatively slow pressure decline. Nucleation and subsequent phase growth play a key role in both processes. An important difference is that solution gas drive involves a binary system and it is controlled by mass transfer, while internal steam drive is fundamentally a single-component system, controlled by heat transfer. In two recent publications (Tsimpanogiannis and Yortsos, 2001a,b) we developed a comprehensive effective continuum model to model solution gas-drive under various conditions. In this report, we extend that approach to the specific problem of internal steam drive.

As discussed in Tsimpanogiannis and Yortsos (2001a,b), the effective continuum model is best suited during the early part of the process, where nucleation and the early stages of bubble growth are dominant. The latter two, particularly the nucleation sequence, are the

main areas of interest of this report. We focus on the effect of the nucleation characteristics on the maximum supersaturation and the nucleation fraction (and the critical gas saturation) and provide an analysis of the effect of various parameters, such as pressure decline rate, on these quantities. Results for the gas phase growth following the conclusion of nucleation are also presented. It is assumed that the pressure decline rates are sufficiently slow so that inertia and spatial gradient effects on bubble growth are negligible. Under the same conditions, the model can in principle be applied to describe the onset of boiling in porous media, driven by the application of a constant heat flux. This application is left for a future study, however.

At later stages of bubble growth, where the various gas clusters compete with each other through a combination of pore geometrical and topological effects, the present continuum model will have obvious drawbacks. In the latter stages, a pore-network model should instead be used. Pore-network models of bubble growth in single-component systems, driven by heat transfer w ere developed by Satik and Yortsos (1996). In principle, these contain all the necessary physics for a rigorous modeling of the process, particularly when significant spatial gradients develop. Such an effort can be pursued in parallel.

The report is organized as follows: First, we formulate the problem closely following Tsimpanogiannis and Yortsos (2001a,b). A scaling analysis of the resulting equation allows to recast the problem in a more useful form, to be used for direct predictions. The numerical results are analyzed. It turns out that for their interpretation, a simplified model of the nucleation and growth periods can be developed. We use the simpler model to obtain expressions for the maximum supersaturation as a function of geometric, thermodynamic and process parameters. This allows us to obtain useful relations for the dependence of the final nucleation fraction (and the critical gas saturation) on process parameters. The theoretical predictions are then compared against experimental results.

II. MATHEMATICAL FORMULATION

Consider an effective porous medium occupied by a single-component liquid. At the beginning of the process, the system is subcooled at the initial temperature, T_o, and pressure, P_o, where $P_o > P^{sat}(T_o)$ and $P^{sat}(T)$ denotes the equilibrium vapor pressure at temperature T. In the practical application discussed by Dehghani and Kamath (1999) this state is achieved by steam injection, followed by steam condensation. Then, the pressure of the system is slowly decreased. Nucleation and subsequent bubble growth are driven by the continuous increase in the supersaturation, $P^{sat}(T_\infty) - P_l(t)$, where T_∞ is the far-field system temperature and subscript l denotes liquid. To describe phase equilibria, we will assume a Clausius-Clapeyron equation

$$\frac{d\ln\left[P^{sat}(T_\infty)\right]}{dT_\infty} = \frac{L_v}{R_g T_\infty^2} \tag{1}$$

where R_g is the ideal gas constant and L_v the molar latent heat of vaporization. Equation (1) does not include Kelvin vapor pressure lowering effects. However, these can be readily incorporated by replacing L_v in (1) by $L_v + P_c v_m$, where P_c is the capillary pressure and v_m the molar liquid volume. More complex thermodynamics can certainly be incorporated (Reid et al., 1986), but the salient features are manifested with the simpler model (1). Conversely, at a specified liquid pressure, P_l, a degree of superheat is present in the system, given by the difference

$$\Delta T = T_\infty - T^{sat}(P_l) \tag{2}$$

where $T^{sat}(P_l)$ denotes the equilibrium temperature corresponding to P_l. The change in supersaturation (or superheat) is here driven by a constant rate of pressure decline. As mentioned, we will proceed with the assumption that the rate of decline is sufficiently slow, so that inertia effects as well as effects of spatial gradients (gravitational and/or viscous) are negligible. This requires sufficiently small Rayleigh, Bond, capillary and Peclet numbers. Instead, emphasis will be placed on nucleation and on the effect of the increase of supersaturation on the growth of the gas phase.

a. Nucleation

As the liquid pressure declines, nucleation sets in. Yortsos and Parlar (1989) reviewed the gas-liquid phase change in porous media and concluded that heterogeneous nucleation is the most plausible mechanism under sufficiently slow rates of supersaturation. In one model, nucleation occurs when a gas bubble, either pre-existing or nucleated inside a cavity at the pore walls, becomes unstable and detaches or otherwise occupies the host pore body. This type of mechanism is in agreement with visual observations from micromodel experiments in solution gas drive (Li and Yortsos, 1995a, El Yousfi et al., 1991, 1997, Bora et al., 2000 and Dominguez et al., 2000) and will also be assumed here. In the cavity model, the activation of a nucleation site occurs when the trapping capillary forces are overcome for the first time. Then, the following condition is satisfied between the radius of the nucleation cavity, r_c, and the (local) supersaturation,

$$P_c \equiv \frac{2\gamma\cos\theta^*}{r_c} = P^{sat}(T_\infty) - P_l(t) \tag{3}$$

where θ^* is the contact angle ($0 < \theta^* < \pi/2$). In the present model, the onset of nucleation is not kinetically related to the degree of supersaturation, as for example, in conventional

approaches for solution gas drive (Firoozabadi and Kaschiev, 1997), but rather depends on the size distribution, $\alpha_c(r_c)$, of the nucleation cavities.

Consider, now, the activation of nucleation sites. With the decrease in the liquid pressure, the right-hand side of (3) increases, eventually becoming positive. Then, various cavities satisfying (3) become activated and their corresponding host pore bodies are occupied by gas. At any time, the current nucleation fraction, f_q, defined as the number fraction of pores that contain sizes which have been activated, is

$$f_q = \int_{r_c}^{\infty} \alpha_c(r) dr \tag{4}$$

where r_c is an implicit function of time, through (3). Equation (4) implies a zero nucleation fraction at zero supersaturation ($r_c \to \infty$) and a nucleation fraction of one at infinite supersaturation ($r_c \to 0$). As elaborated in Tsimpanogiannis and Yortsos (2001a), the cavity size distribution, α_c, pertains only to the largest cavity in any given pore (as this cavity will be activated first). Also, equation (4) slightly overestimates the true nucleation fraction, since pores containing sites to be activated later, may already be occupied by gas, due to the growth of gas clusters from neighboring pores. However, in most cases, nucleation terminates well before gas bubble growth has occurred to any substantial degree ($S_g \ll 1$), thus (4) should be an excellent approximation.

It is apparent that f_q will have a different dependence on parameters, depending on the assumed cavity size distribution. In the present report, we will consider distribution of the Rayleigh type,

$$f_q = \exp\left(-\frac{\pi r_c^2}{4 r_c^{*2}}\right) = \exp\left[-\frac{\pi \gamma^2}{r_c^{*2}[P^{sat}(T_\infty) - P_l]^2}\right] \tag{5}$$

where r_c^* is a characteristic (here the mean) cavity size, as well as a stretched-exponential

$$f_q = \exp\left(-\frac{r_c^n}{\sigma r_c^{*n}}\right) \tag{6}$$

where n is a positive exponent and σ is a measure of the variance. The type of distribution influences significantly the results to be obtained, as will be demonstrated below.

As long as the level of supersaturation increases with time, the right-hand-side of equation (5) also increases, implying that additional sites become activated, and the nucleation fraction continuously rises. This is consistent with experimental evidence of sequential nucleation reported by Satik and Yortsos (1996). After the supersaturation reaches a maximum (local or global), equation (5) predicts a decreasing f_q, which is unphysical. Therefore, in segments of decreasing supersaturation the nucleation fraction is assumed constant. When the supersaturation goes through a global maximum, it signals the end of the nucleation period, in which case the fraction of pores ultimately activated, f_{qf}, will be given by equations

(5) or (6) at the time of the maximum supersaturation. We note that in typical solution gas-drive experiments, f_{qf} is very small, of the order of $10^{-9} - 10^{-6}$.

Through this process, nucleation centers are activated sequentially, giving rise to evolving gas clusters, which grow by heat transfer from the liquid to the gas. Sequential nucleation results into clusters of different ages (the time passed since a particular class of gas clusters has been nucleated/activated). Let $\omega(\tau)$ be the number density of clusters nucleated per total number of pores. Then, $\omega(\tau)d\tau$ is the number of new clusters per total number of pores that become activated in the time interval between τ and $\tau + d\tau$. Evidently,

$$\omega(\tau)d\tau = df_q \tag{7}$$

This relation will be used below to simplify the expressions for the gas phase growth.

b. Gas phase growth

During the growth of the gas phase we can roughly distinguish two periods, one in which the growth is within single pores and another corresponding to gas clusters spanning several pores (Tsimpanogiannis and Yortsos, 2001a). The first period extends throughout and following the nucleation stage, the second is the later stage of growth. In either, growth is driven by heat transfer. In general, different clusters compete for the available heat in the liquid, the relative heat transfer rates depending on their geometry and relative position.

In the absence of competition between adjacent clusters and under the assumption that heat transfer is conduction-controlled (namely that the Peclet number is sufficiently small), an isolated cluster j grows at a rate which is proportional to its effective radius, $R_j(t,\tau)$, and the driving force $T_\infty - T^{sat}(P_l)$ where T_∞ is the far-field temperature. This is true even for ramified fractal clusters, as was verified by Satik and Yortsos (1996) for a percolation cluster. Assuming that the gas is ideal, we can write the following mass balance for a growing cluster

$$\left(\frac{M_w}{R_g T_g}\right)\frac{d}{dt}\left[(P_l + P_c)V_g\right] \approx 4\pi R_j \frac{k_{eff}}{\tilde{L}_v}(T_\infty - T^{sat}(P_l)) \tag{8}$$

where M_w is the molecular weight of the gas, T_g the temperature in the gas phase, V_g the gas cluster volume, k_{eff} an effective conductivity and $\tilde{L}_v$ the mass latent heat of vaporization ($L_v = \tilde{L}_v M_w$). In equation (8) we have also included the capillary pressure, P_c, which in the application of interest can be significant. To simplify, we linearize the phase equilibria around P_o,

$$T^{sat}(P_l) \approx T^{sat}(P_o) + \frac{dT^{sat}}{dP}(P_l - P_o) \tag{9}$$

and take without significant loss $T_g \approx T_o$.

The gas volume V_g takes a different expression in the two different periods (Tsimpanogiannis and Yortsos, 2001a). For growth within a single pore, $V_g \approx V_c \left(\frac{R_j}{r_c^*}\right)^3$, where V_c is a characteristic cavity volume (defined here as $\frac{4}{3}\pi r_c^{*3}$). For growth of a cluster spanning several pores, we have $V_g \approx A^* V_s \left(\frac{R_j}{r_s^*}\right)^{D_f}$, where V_s is the average site volume, r_s^* is a characteristic pore body size, D_f is the mass fractal dimension, equal approximately to 2.5 for a 3-D cluster, and A^* is a dimensionless geometric prefactor. To capture both periods with the same equation we write

$$\left(\frac{AV_cM_w}{R_gT_o}\right)\frac{d}{dt}\left[(P_l+P_c)\left(\frac{R_j}{r_c^*}\right)^{D_f}\right] = 4\pi R_j \frac{k_{eff}}{\tilde{L}_v}(T_\infty - T^{sat}) \tag{10}$$

with the understanding that D_f varies between 3 and 2.5, and A between 1 and $A = \frac{A^*V_s}{V_c}\left(\frac{r_c^*}{r_s^*}\right)^{D_f}$, during the nucleation period and growth periods, respectively.

Under the above assumptions, the gas phase will be described as a collection of clusters of size $R(t,\tau)$, the dynamics of each of which is described by equation (10), with R_j replaced by R, namely

$$\left(\frac{AV_cM_w}{R_gT_o}\right)\frac{\partial}{\partial t}\left[(P_l+P_c)\left(\frac{R}{r_c^*}\right)^{D_f}\right] = 4\pi R \frac{k_{eff}}{\tilde{L}_v}(T_\infty - T^{sat}) \tag{11}$$

subject to the initial condition $R(\tau,\tau) = r_c(\tau)$, where r_c satisfies (3).

Consider, next, the heat balance for the entire system. We have

$$\begin{aligned} V_p\left[\phi(1-S_g)\rho_l C_{pl} + (1-\phi)\rho_r C_{pr}\right]\frac{dT_\infty}{dt} = & - 4\pi\phi k_{eff}(T_\infty - T^{sat})N_T\int_0^t R(t,\tau)\omega(\tau)d\tau \\ & + hA_{surf}(T_o - T_\infty) \end{aligned} \tag{12}$$

where the integration is over all existing clusters, C_p denotes heat capacity per unit mass, ϕ is porosity, h is the heat transfer coefficient to the surroundings, assumed at temperature T_o, and A_{surf} is the corresponding surface area through which heat is exchanged.

The gas saturation is related to the radius of the growing clusters and the nucleation fraction through the relation

$$S_g = Av\int_0^{f_q}\left(\frac{\hat{R}(t,f_q)}{r_c^*}\right)^{D_f} df_q \tag{13}$$

where we introduced the volume ratio $v \equiv \frac{V_c}{V_s}$ and the notation $\hat{R}(t,f(\tau)) \equiv R(t,\tau)$, for the radius of a cluster at time t, nucleated when the nucleation fraction was $f(\tau)$. Note that the liquid mass balance can also be expressed and reads as

$$\frac{Q(t)}{V_p} = -(1-S_g)c\frac{dP_l}{dt} + \frac{dS_g}{dt} \tag{14}$$

where c takes values in the range of $1.45 \times 10^{-4} - 1.45 \times 10^{-3}\text{MPa}^{-1}$. However, in the present problem it is not used. Subject to the relevant initial conditions, the system of equations (11), (12), (14) and (13) can be integrated. Integration proceeds until the time when the critical gas saturation is reached. In the present approach, we assume that the critical gas saturation, S_{gc}, can be predicted given the nucleation fraction and the capillary and Bond numbers (Du and Yortsos, 1999, Tsimpanogiannis and Yortsos, 2001a,b, Tsimpanogiannis and Yortsos, 2002). Therefore, for the purposes of estimating S_{gc}, it only suffices to model well the events during the nucleation period.

c. Dimensionless formulation and scaling

For the solution of the problem, we recast the equations in dimensionless form. Denote dimensionless quantities by subscript D and scale temperature by T_o, pressure by P_o, cluster size by r_c^*, and time by $t^* = \frac{P_o}{a}$, where a is the constant pressure decline rate. The dimensionless mass balance for the gas phase is given by

$$(1 - t_D + \Pi_c)\frac{\partial \hat{R}_D^{D_f}}{\partial t_D} = \frac{\Pi_2}{A\Pi_1}(T_{D\infty} - T_D^{sat})\hat{R}_D + \hat{R}_D^{D_f} \tag{15}$$

while the dimensionless heat balance for the system reads

$$\begin{aligned}(1 - S_g)\left(\Pi_\rho + \frac{1-\phi}{\phi}\right)\frac{dT_{D\infty}}{dt_D} = & - \frac{1}{\Pi_1}(T_{D\infty} - T_D^{sat})\int_0^{f_q} \hat{R}_D(t_D, f_q)df_q \\ & + \Pi_H(1 - T_{D\infty})\end{aligned} \tag{16}$$

In the above, we have defined the dimensionless groups

$$\begin{aligned}\Pi_1 &= \frac{V_s\rho_r C_{pr} a}{4\pi P_o k_{eff} r_c^*} = \frac{V_p\rho_r C_{pr} a}{4\pi P_o N_T k_{eff} r_c^*}, \\ \Pi_2 &= \frac{R_g T_o^2}{\upsilon M_w \tilde{L}_v}\frac{\rho_r C_{pr}}{P_o}, \qquad \Pi_H = \frac{hA_{surf}P_o}{V_p\rho_r C_{pr} a\phi}, \\ \Pi_\rho &= \frac{\rho_l C_{pl}}{\rho_r C_{pr}} \quad \text{and} \quad \Pi_c = \frac{2\gamma\cos\theta^*}{r_c^* P_o}\end{aligned} \tag{17}$$

Parameter Π_1 expresses the ratio of the characteristic times for heat diffusion at the pore scale to that for the decline of pressure. Although a small number in typical applications, it plays a key role in determining the nucleation fraction and the critical gas saturation.

In addition, we have the following relations: The gas saturation is

$$S_g = A\upsilon \int_0^{f_q} \hat{R}(t_D, f_q)^{D_f} df_q \tag{18}$$

Using the linearized phase equilibria, the dimensionless superheat is

$$\theta \equiv T_{D\infty} - T_D^{sat} = T_{D\infty} - (1 - \psi t_D) \tag{19}$$

where $\psi \equiv \frac{R_g T_o}{L_v}$ or $\psi \equiv \frac{R_g T_o}{L_v + P_c v_m}$, when Kelvin effects are important. The cavity size that becomes activated at a given time and temperature can be expressed in terms of the supersaturation

$$s \equiv P_D^{sat}(T_{D\infty}, t_D) - P_{Dl}(t_D) = t_D - \frac{1 - T_{D\infty}}{\psi} \tag{20}$$

or, more conveniently, in terms of the rescaled supersaturation

$$s_D \equiv \frac{s}{\Pi_c} \tag{21}$$

Then, the nucleation fraction is

$$f_q = \exp\left(-\frac{\pi}{4 s_D^2}\right), \quad f_q = \exp\left(-\frac{1}{\sigma s_D^n}\right) \tag{22}$$

depending on the size distribution used. In the solution of the problem, we assumed that the process begins ($t_D = 0$) when the pressure is at the bubble point corresponding to T_o. Initial conditions for the simulations were $T_{D\infty} = 1$, $P_{Dl} = 1$ and $R_D(\tau, \tau) = s_D^{-1}(\tau)$.

The above system contains one key parameter, Π_1, describing the effect of the rate of increase of the supersaturation. Because it is small, a further rescaling of the nucleation fraction and the cluster size is necessary. After some analysis (Tsimpanogiannis and Yortsos, 2001a), it is not difficult to show that for the cavity nucleation model, the following scaling is valid, $f_q \sim \Pi_1^{\frac{D_f}{D_f - 1}}$ and $f_q R^{D_f} \sim O(1)$ (where, given that the nucleation fraction varies only during the first period, $D_f = 3$). This scaling contains the main effect of the pressure decline rate on the nucleation fraction. Thus, we define a rescaled nucleation fraction and rescaled cluster sizes

$$\phi_q = f_q \Pi_1^{-\frac{3}{2}} \quad \text{and} \quad \rho_D = \Pi_1^{\frac{1}{2}} \hat{R}_D \tag{23}$$

In this notation, the governing equations become

$$(1 - t_D + \Pi_c) \frac{\partial \rho_D^{D_f}}{\partial t_D} = \frac{\Pi_2}{A} \theta \rho_D + \rho_D^{D_f} \tag{24}$$

and

$$(1 - S_g) \left(\Pi_\rho + \frac{1 - \phi}{\phi}\right) \frac{dT_{D\infty}}{dt_D} = -\theta \int_0^{\phi_q} \rho_D(t_D, \phi_q) d\phi_q + \Pi_H (1 - T_{D\infty}) \tag{25}$$

while

$$S_g = Av \int_0^{\phi_q} \rho(t_D, \phi_q)^{D_f} d\phi_q \tag{26}$$

The numerical solution of the system of the rescaled equations is described below.

III. NUMERICAL RESULTS

The system of differential equations was solved numerically using a fourth-order Runge-Kutta method (Press et al., 1994). At each time step we examine whether nucleation of a new class of gas clusters is possible, namely whether the supersaturation is increasing. If so, a new class of gas clusters is added. Then, the simultaneous growth of all different classes of clusters is computed. When the supersaturation reaches a maximum, further nucleation stops. In the typical case, parameters which can vary over a significant range are Π_1 and Π_c (and possibly Π_2). An additional important variable is the type of the cavity size distribution used in the calculation of the nucleation fraction. The sensitivity to these parameters was examined in the simulations.

The effect of Π_1 and Π_c on the rescaled nucleation fraction, ϕ_q, the mean rescaled radius, $\rho_{D,m}$, the rescaled supersaturation, s_D, and the gas saturation, S_g, is shown in Figs. 1-4. In these calculations, we used a stretched exponential ($n = 1.0$ and $\sigma = 1.0$) cavity size distribution, Π_2 was kept constant to the value 0.9697×10^8, we assumed an adiabatic system ($\Pi_H = 0$), while Π_1 varied over several orders of magnitude (from 10^{-14} to 10^{-5}).

The variation of ϕ_q as a function of the dimensionless time, t_D, and of the parameters Π_1 and Π_c is shown in Fig. 1. The nucleation fraction increases rapidly in a small time interval, and then stabilizes to a final value at the conclusion of nucleation. Such behavior is characteristic of nucleation processes, and has features similar to those reported by Tsimpanogiannis and Yortsos (2001a, b) for solution gas drive. There is a slight effect of Π_1, which basically demonstrates the correctness of the scaling (23). The effect of Π_c is significant. As Π_c increases, the final nucleation fraction ϕ_{qf} (hence f_{qf}) decreases, while the onset of nucleation is delayed (Fig. 1b). The increase of f_{qf} with an increase in Π_1 and a decrease in Π_c is expected. Larger values of Π_1 result from a faster decline rate, a greater departure from equilibrium, the establishment of a greater supersaturation in the system, hence the activation of more nucleation sites. Likewise, smaller Π_c imply that nucleation is facilitated at increasingly smaller supersaturations, as larger size cavities can be activated more easily.

Fig. 2 shows the corresponding effects on the mean rescaled size ρ_{Dm}. There are two different regions, corresponding to the nucleation period, and another to growth after nucleation. The first period can be approximated as a linear function of time. The effect of Π_1 is

relatively insignificant at small Π_1, confirming the validity of the scaling (23). The effect of Π_c (not shown) is more significant. Smaller values of Π_c lead to an increase in the nucleation fraction, and a corresponding decrease in the size of the gas clusters at the conclusion of nucleation.

Fig. 3 shows plots of the rescaled supersaturation s_D as a function of time for different Π_1 and Π_c. During the nucleation period (straight line segment in Fig. 3a), the supersaturation increases with time almost linearly, suggesting that $T_{D\infty}$ does not vary significantly in that period. Eventually, the rate of supersaturation increase slows down and, at some point, s_D reaches a maximum, s_{Dm}, at which point nucleation terminates. Following this point, the supersaturation decreases monotonically. The maximum value s_{Dm} is plotted in Fig. 3b as a function of Π_1 for two different values of Π_c. Note that s_{Dm} is in general of the order of $10^{-3} - 10^{-1}$. The dependence on the parameters becomes stronger at larger Π_1 and smaller Π_c.

The evolution of the gas saturation is shown in Fig. 4. It follows that of f_q, during the nucleation period, and that of ρ_{Dm}, during the period of growth. The effect of Π_c is indirect, in that smaller values of Π_c promote larger values of S_g due to an increase in both f_{qf} and ρ_D. All these trends are similar to the case of solution gas drive, as explained in Tsimpanogiannis and Yortsos (2001a, b). We refer the reader to these publications for other effects, including the effect of Π_1 and Π_c on the critical gas saturation S_{gc}. Because the latter pertains to the formation of a sample-spanning cluster, in the absence of viscous or gravity effects, S_{gc} actually reflects the variation of f_{qf}. Thus, S_{gc} can be considered a power-law both of Π_1 and of Π_c with exponents that vary between 0.16 and 0.25 with respect to Π_1 and between -0.33 and -0.22, with respect to Π_c, respectively (see Tsimpanogiannis and Yortsos, 2001a, b).

The effect of Π_H on the rescaled nucleation fraction, ϕ_q and the gas saturation, S_g, is shown in Figs. 5-6. In these calculations, we used a stretched exponential ($n = 0.2233$ and $\sigma = 0.1364$) cavity size distribution. As Π_H increases, the level of superheat and thus the level of the supersaturation in the system is higher. This leads to an earlier onset of nucleation, as well as a higher degree of nucleation. Note, however, that the effect of Π_H on the maximum superheat and on the rescaled final nucleation fraction, ϕ_{qf}, is not significant. A change of Π_H by three orders of magnitude, results in a change of ϕ_{qf} by a factor of less than 2. The gas saturation increases faster as the heat transfer coefficient increases. This is due to the maintaining of a higher level of superheat, therefore a larger driving force for gas volume growth. Interestingly, as the heat transfer coefficient decreases the gas saturation growth slows down at larger values of the gas saturation. A noticeable difference, however, at higher values of Π_H, is that the superheat is not be completely depleted before the gas saturation becomes equal to one, as happens with the lower values of Π_H.

The numerical solutions obtained will be compared against available experimental results. However, before doing so it is beneficial to provide an interpretation of the numerical findings, using a simpler model.

IV. INTERPRETATION USING A SIMPLER MODEL

To interpret the results obtained we will consider a simpler model that captures the essential features of the problem, just like in Tsimpanogiannis and Yortsos (2001a, 2001b). Consider, first, the nucleation period.

a. Nucleation

We use the following equations for the gas phase growth and the superheat

$$(1+\Pi_c)\frac{\partial \rho_D^3}{\partial t_D} \approx \Pi_2 \theta \rho_D \tag{27}$$

and

$$\left(\Pi_\rho + \frac{1-\phi}{\phi}\right)\frac{d\theta}{dt_D} \approx \psi\left(\Pi_\rho + \frac{1-\phi}{\phi}\right) - \theta\int_0^{\phi_q(s)} \rho_D d\phi_q + \Pi_H(\psi t_D - \theta) \tag{28}$$

These are subject to the initial conditions

$$\theta(0) = 0 \quad \text{and} \quad \rho_D(\tau,\tau) = \frac{\Pi_1^{\frac{1}{2}}}{s_D(\tau)} \tag{29}$$

At early times and for small Π_1, the solution is approximately

$$\theta \approx \psi t_D \quad \text{and} \quad \rho_D \approx \left[\frac{\Pi_2}{3(1+\Pi_c)}\frac{\theta^2}{\psi}\right]^{\frac{1}{2}} \tag{30}$$

Note that the heat transfer term does not affect the early behavior (compare also with Figs. 5-6). The dimensionless superheat is linearly proportional to the dimensionless time and the mean cluster size becomes evantually proportional to time. Both are consistent with the numerical results during the nucleation period (Figs. 2 and 3).

We will use (28) to approximate the approach to the maximum superheat. The latter is reached when $\frac{d\theta}{dt_D} = 0$, namely when

$$\theta\int_0^{\phi_q} \rho_D d\phi_q \approx \left(\Pi_\rho + \frac{1-\phi}{\phi}\right)\psi \tag{31}$$

Following a similar approach as in Tsimpanogiannis and Yortsos (2001a, b) we can combine (30) and (30) with the definition of ϕ_q to obtain an approximate algebraic equation for the rescaled maximum supersaturation, s_{Dm}. For example, for the case of Rayleigh distribution we have the equation

$$\frac{\pi}{4s_{Dm}^2} - 2\ln s_{Dm} \approx \frac{1}{2}\ln\psi - \ln\left(\Pi_\rho + \frac{1-\phi}{\phi}\right) - \frac{1}{2}\ln 3 - \frac{3}{2}\ln\Delta \tag{32}$$

where we introduced the combination of variables

$$\Delta \equiv \Pi_1 \Pi_c^{-\frac{4}{3}} \left(\frac{\Pi_2}{1+\Pi_c}\right)^{-\frac{1}{3}} \tag{33}$$

Likewise for the case of a stretched exponential we get

$$\sigma^{-1} s_{Dm}^{-n} - 2\ln s_{Dm} \approx \frac{1}{2}\ln\psi - \ln\left(\Pi_\rho + \frac{1-\phi}{\phi}\right) - \frac{1}{2}\ln 3 - \frac{3}{2}\ln\Delta \tag{34}$$

These equations suggest that the dependence of the maximum supersaturation (hence the maximum superheat since $\theta = \psi \Pi_c s_D$) on the various parameters. The solutions of (32) for the Rayleigh distribution and of (34) for two different cases of a stretched exponential are plotted in Fig. 7, as a function of Δ. For the Rayleigh distribution, s_{Dm} varies weakly, in the range $0.1 - 1$, as Δ varies over several orders of magnitude (between 10^{-14} and 10^{-5}). For small Δ, the maximum supersaturation is practically constant. As Δ takes larger values, s_{Dm} increases weakly and eventually much more strongly, as Δ approaches the order of one (compare also with Fig. 3). On the other hand, for the stretched exponential, the variation is much stronger in the logarithmic plot, and almost approximates a straight line. Stronger dependence on Δ is observed for the case when the tail of the cavity size distribution becomes longer (smaller values for n). Plotted in the same figure are also the results of the numerical solution of the full problem for a number of different parameter values. The agreement between the numerical results and the simple analytical model is very good and demonstrates the validity of the simple model.

Equations (32)-(34) can be used to approximate the final nucleation fraction. For all cases we have

$$f_{qf} \approx s_{Dm}^{-2} \Lambda \Pi_1^{\frac{3}{2}} \Pi_c^{-2} \left[\frac{\Pi_2}{3(1+\Pi_c)}\right]^{-\frac{1}{2}} \tag{35}$$

where

$$\Lambda = \left(\Pi_\rho + \frac{1-\phi}{\phi}\right) \psi^{-\frac{1}{2}} \tag{36}$$

The behavior of the maximum supersaturation as a function of the parameter Δ is very similar to that in solution gas drive (Tsimpanogiannis and Yortsos, 2001a, b). In particular,

(a) In the region where s_{Dm} varies weakly with Δ (at very small Δ) the final nucleation fraction varies as a power law of Π_1, with exponent equal to 3/2.

(b) In the region where s_{Dm} may be approximated by a power-law dependence on Δ, e.g. as $s_{Dm} \sim \Delta^m$, we have the scaling

$$f_{qf} \sim \Lambda \Delta^{\frac{3}{2}-2m} \tag{37}$$

Such a dependence on Δ leads to a decrease in the exponent in the power-law scaling of f_{qf} on Π_1. For example, if we take $m \approx 1/4$ (a value examined in more detail in Tsimpanogiannis and Yortsos, 2001a, b), we read

$$f_{qf} \sim \Pi_1 \qquad \text{and} \qquad f_{qf} \sim r_c^* \tag{38}$$

b. Gas cluster growth

The modeling of the growth regime, where nucleation has terminated, can be simplified if we consider only one class of clusters and simplify the heat and mass balances as follows

$$\frac{d\theta}{dt_D} \approx \frac{-\theta z + \Pi_H(\psi t_D - \theta)}{(\Pi_\rho + \frac{1-\phi}{\phi})(1 - \upsilon \Pi_2 k_1 z^{D_f})} + \psi \tag{39}$$

and

$$\frac{dz^{D_f}}{dt_D} = \frac{k_1^{-1}\theta z + z^{D_f}}{(1 - t_D + \Pi_c)} \tag{40}$$

Here, we introduced the variable

$$z \equiv \phi_{qf} \rho_D \tag{41}$$

and the parameter

$$k_1 = \frac{\phi_{qf}^{1-D_f}}{\Pi_2} \tag{42}$$

The final value of the rescaled nucleation fraction, ϕ_{qf}, as well as initial values for $T_{D\infty}$ and ρ_D needed for the above calculation, are obtained from the previous analysis.

V. COMPARISON WITH EXPERIMENTS

The theoretical model was next compared to the experimental results of Dehghani et al. (1997). In these experiments, the pressure at the open end of a Colton sandstone core, saturated with water and embedded in a constant temperature bath, was slowly reduced at the rate of 0.7448 bar/h (10.8 psi/h). The other end of the core was kept closed to flow. Properties of the core of interest to this report were taken as follows: $r_s = 3.0 \times 10^{-5}\ cm$, $r_c = 3.0 \times 10^{-7}\ cm$. Additional physical parameters and values of the dimensionless parameters used in the calculations are shown in Table 1.

The gas saturation as a function of time for the single-component experiment and for various axial positions along the core are shown in Fig. 8. It is worth noting that the evolution of the gas saturation is slower as the distance from the entrance of the core increases. In a way, this reflects a reduced rate of pressure decline, or a decrease in the heat transfer coefficient as the distance from the open end increases. For a better comparison of the data, we attempted to collapse all data into a single curve. By replotting the data using as time origin the time the boiling point in the bulk is reached (which is $t_o = 84$ minutes), and by rescaling time by a factor $b(L)$, where L is the distance from the open end, we were able to collapse satisfactorily all data in a single curve, as shown in Fig. 9. The less satisfactory collapse of the data at the early times could be the result of poor CT-scan resolution in the low porosity sandstone used in the experiments (Dehghani et al., 1997). The variation of the factor $b(L)$ which allows this collapse is shown in Fig. 10. It is a linear function of the dimensionless distance and the best fit line describing the data is given by: $b(L) = 1.0106 + 5.1513\left(\frac{L}{L_o}\right)$, where L_o is the core length. We then attempted to match this universal curve using our model. As shown in Fig. 9, a very good match was obtained, using a stretched exponential cavity size distribution with $n = 0.35$ and $\sigma = 1.0$.

VI. CONCLUSIONS

In this report we developed an effective continuum model to describe the nucleation and subsequent growth of a gas phase from a supersaturated liquid in a porous medium, driven by heat transfer. The evolution of the gas results from the reduction of the system pressure at a constant rate. The model addresses two stages before the onset of bulk gas flow, nucleation and gas phase growth.

We used heterogeneous nucleation models in the form of pre-existing gas, trapped in hydrophobic cavities to investigate the nucleation behavior. Using scaling analysis and a simpler analytical model we showed that the relevant quantities during nucleation can be expressed in terms of a simple combination of dimensionless parameters, which include rate

effects. The subsequent evolution of the gas phase were also described using numerical and analytical models.

The theory predicts that the maximum supersaturation in the system is a weakly increasing function of the decline rate. This function depends sensitively on the probability density function of the nucleation cavity sizes. It also predicts that the final nucleation fraction, thus the critical gas saturation, is a power law of the decline rate. The theory was then compared with available experimental data of internal steam drives, such as the blowdown experiments in carbonate rocks (Dehghani et al., 1997) and a good match is obtained by appropriate fitting of the nucleation characteristics of the medium.

References

[1] Bora, R., Maini, B.B., and A. Chakma, "Flow Visualization Studies of Solution Gas Drive Process in Heavy Oil Reservoirs Using a Glass Micromodel," *SPE Reservoir Eval. Eng.*, **3**, 224-229 (2000).

[2] Dehghani, K., Kumar, M., deZabala, E.F., Meyer, R.F., and H. Duran, "An Experimental and Numerical Study of In-Situ Stemadrive During Cyclic Steaming," *SPERE*, 144-150 (May 1997).

[3] Dehghani, K., and J. Kamath, "High Temperature Blow-Down Experiments in a Vuggy Carbonate Core," paper *SPE 56542* presented at the SPE Annual Technical Conference and Exhibition, Houston, TX (3-6 October 1999).

[4] Dominguez, A., Bories, S., and M. Prat, "Gas Cluster Growth by Solute Diffusion in Porous Media. Experiments and Automaton Simulation on Pore Network," *Int. J. Moultiphase Flow*, **26**, 1951-1979 (2000).

[5] Du, C., and Y.C. Yortsos, "A Numerical Study of the Critical Gas Saturation in a Porous Medium," *Transport in Porous Media*, **35**, 205-225 (1999).

[6] El Yousfi, A., Zarcone, C., Bories, S. and R. Lenormand, "Mècanismes de Formation d'une Phase Gazeuse par détente d'un liquide en Milieu Poreux," *C.R. Acad. Sci. Paris, Série II,* **313**, 1093-1098 (1991).

[7] El Yousfi, A., Zarcone, C., Bories, S. and R. Lenormand, "Physical Mechanisms for Bubble Growth During Solution Gas Drive," paper *SPE 38921* presented at the SPE Annual Technical Conference and Exhibition, San Antonio, TX (5-8 October 1997).

[8] Firoozabadi, A., and D. Kashchiev, "Pressure and Volume Evolution During Gas Phase Formation in Solution Gas Drive Processes," *SPE Journal*, **1**, 219-227 (1997).

[9] Li, X., and Y.C. Yortsos, "Visualization and Simulation of Bubble Growth in Pore Networks," *AIChE J.*, **41**, 214-222 (1995a).

[10] Li, X., and Y.C. Yortsos, "Theory of Multiple Bubble Growth in Porous Media by Solute Diffusion," *Chem. Eng. Sci.*, **50**, 1247-1271 (1995b).

[11] Press, W.H., Teukolsky, W.T., Vettering, S.A., and B.P. Flannery, *Numerical Recipies,* 2nd ed. Cambridge University Press, (1992).

[12] Reid, R.C., Prausnitz, J.M., and B.E. Poling, *The Properties of Gases and Liquids,* 4th ed. McGraw-Hill, New York, (1986).

[13] Satik, C., and Y.C. Yortsos, A Pore Network Study of Bubble Growth in Porous Media Driven by Heat Transfer," *ASME J. of Heat Transfer*, **118**, 155-462 (1996).

[14] Tsimpanogiannis, I.N., and Y.C. Yortsos, "An Effective Continuum Model for the Liquid-to-Gas Phase Change in a Porous Medium Driven by Solute Diffusion: I. Constant Pressure Decline Rates," paper *SPE 71502* presented at the SPE Annual Technical Conference and Exhibition, New Orleans, LA (30th September-3rd October 2001); also AIChEJ, submitted (2001a).

[15] Tsimpanogiannis, I.N., and Y.C. Yortsos, "An Effective Continuum Model for the Liquid-to-Gas Phase Change in a Porous Medium Driven by Solute Diffusion: II. Constant Liquid Withdrawal Rates," AIChEJ, submitted (2001b).

[16] Tsimpanogiannis, I.N., and Y.C. Yortsos, "A Numerical Study of the critical Gas Saturation in a Porous medium in the Presence of Viscous or Gravity Gradients," In preparation (2002).

[17] Yortsos, Y.C., and M. Parlar, "Phase Change in Binary Systems in Porous Media: Application to Solution Gas Drive," paper *SPE 19697*, presented at the SPE Annual Technical Conference and Exhibition, San Antonio, TX (8-11 October 1989).

Parameter	*Value*
$a\ (bar/h)$	0.7448
$C_{pl}\ (J/(KgK))$	5954.7
$C_{pr}\ (J/(KgK))$	850.0
$k\ (\mu m^2)$	4.145×10^{-4}
$k_{eff}\ (W/(mK))$	1.0
$L_o\ (cm)$	11.354
$L_v\ (J/mol)$	37294.8
MW (g/mol)	18.016
$P_o\ (bar)$	9.276
$r_c\ (cm)$	3.0×10^{-7}
$r_s\ (cm)$	3.0×10^{-5}
$T_o\ (K)$	449.4
$\gamma\ (mN/m)$	55.0
Π_1	1.333×10^{-10}
Π_2	9.697×10^{7}
Π_c	3.901×10^{1}
Π_H	2.697×10^{2}
Π_ρ	2.981×10^{0}
$\rho_r\ (Kg/(m^3))$	2350.0
υ	$1. \times 10^{-6}$
ϕ	0.111
ψ	1.002×10^{-1}

Table 1: Characteristic values for the various parameters.

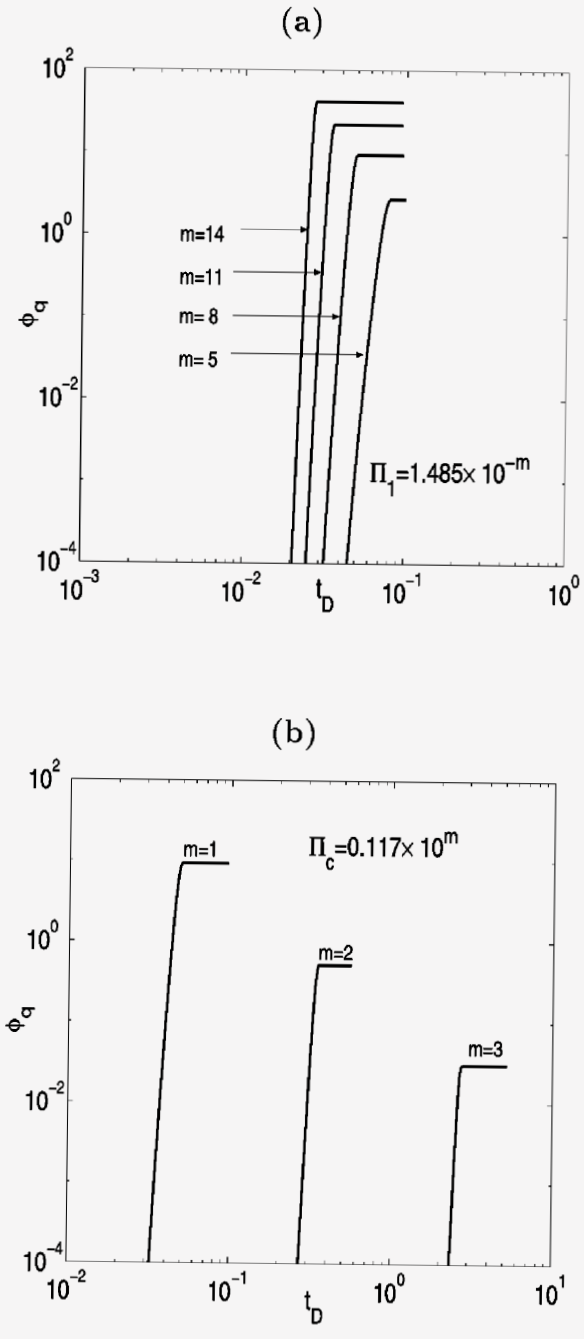

Figure 1: Variation of the rescaled nucleation fraction, ϕ_q, as a function of the dimensionless time, t_D. **(a)** Effect of $\Pi_1 = 1.485 \times 10^{-m}$, for $\Pi_2 = 9.6972 \times 10^7$, $\Pi_\rho = 2.981$ and $\Pi_H = 0$. **(b)** Effect of $\Pi_c = 0.117 \times 10^m$, for $\Pi_1 = 1.485 \times 10^{-8}$, $\Pi_2 = 9.6972 \times 10^7$, $\Pi_\rho = 2.981$ and $\Pi_H = 0$.

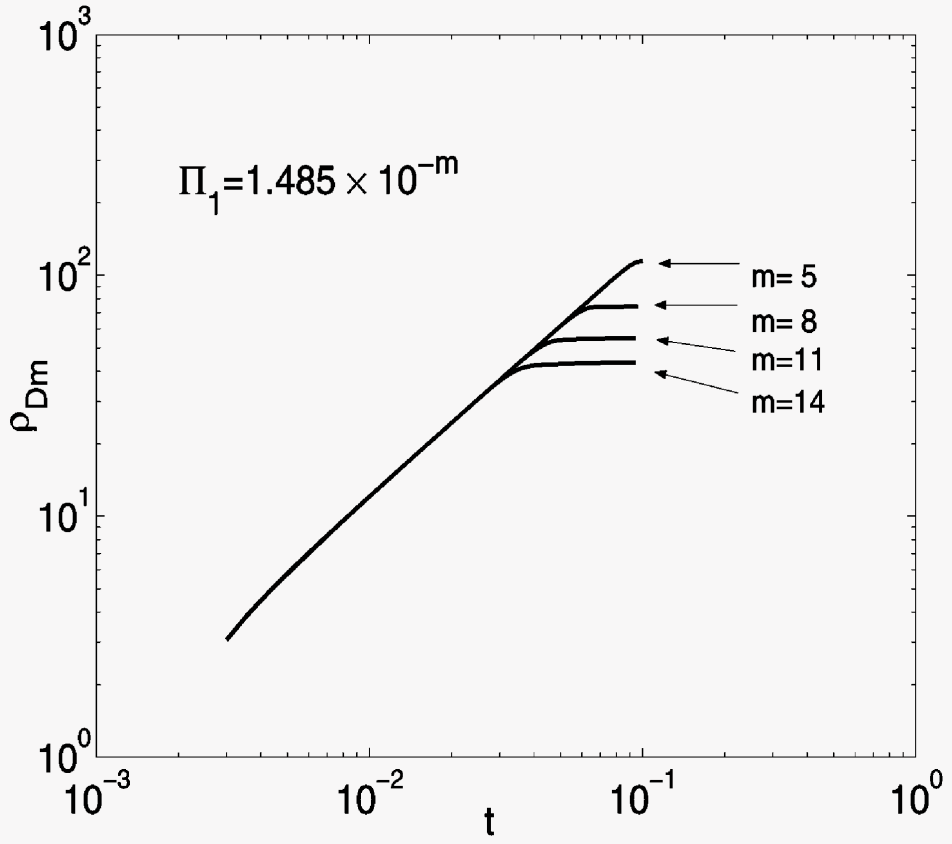

Figure 2: Variation of the mean rescaled dimensionless radius, ρ_{Dm}, as a function of dimensionless time, t_D. Effect of $\Pi_1 = 1.485 \times 10^{-m}$, for $\Pi_2 = 9.6972 \times 10^7$, $\Pi_\rho = 2.981$, $\Pi_c = 0.117 \times 10^1$ and $\Pi_H = 0$.

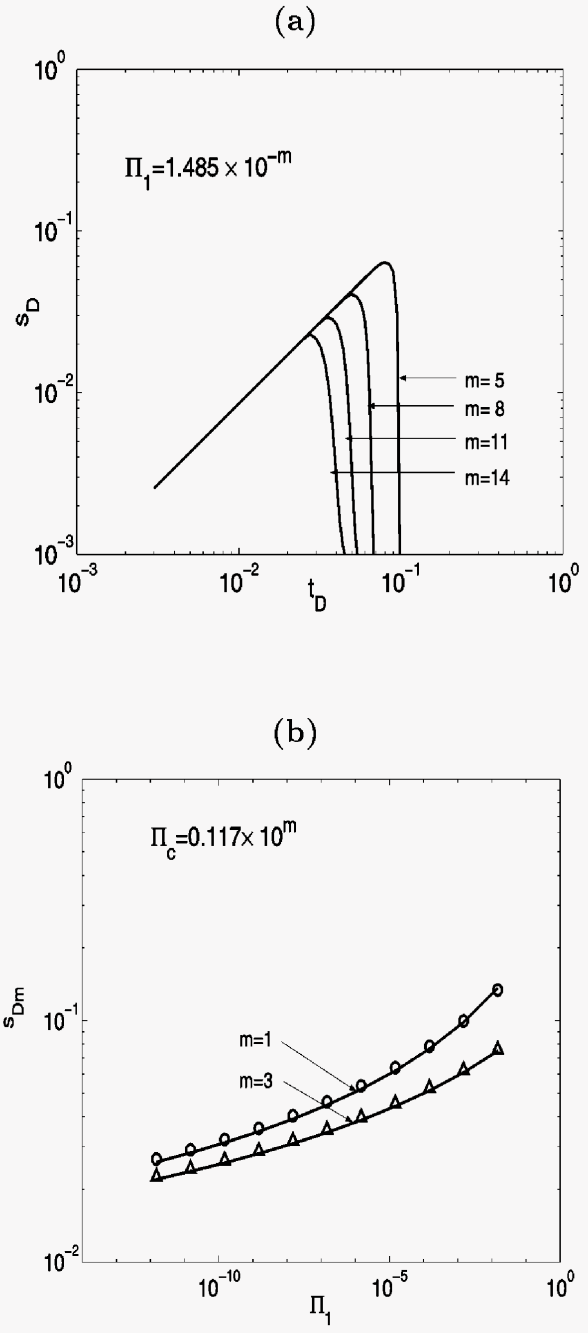

Figure 3: Numerical results for the rescaled supersaturation, s_D: **(a)** Variation as a function of dimensionless time, t_D. Effect of $\Pi_1 = 1.485 \times 10^{-m}$, for $\Pi_2 = 9.6972 \times 10^7$, $\Pi_\rho = 2.981$ and $\Pi_H = 0$. **(b)** Effect of the parameter Π_1 on the maximum rescaled supersaturation, s_{Dm}, for $\Pi_c = 0.117 \times 10^m$. Points correspond to the full numerical solution, solid lines correspond to the simpler problem.

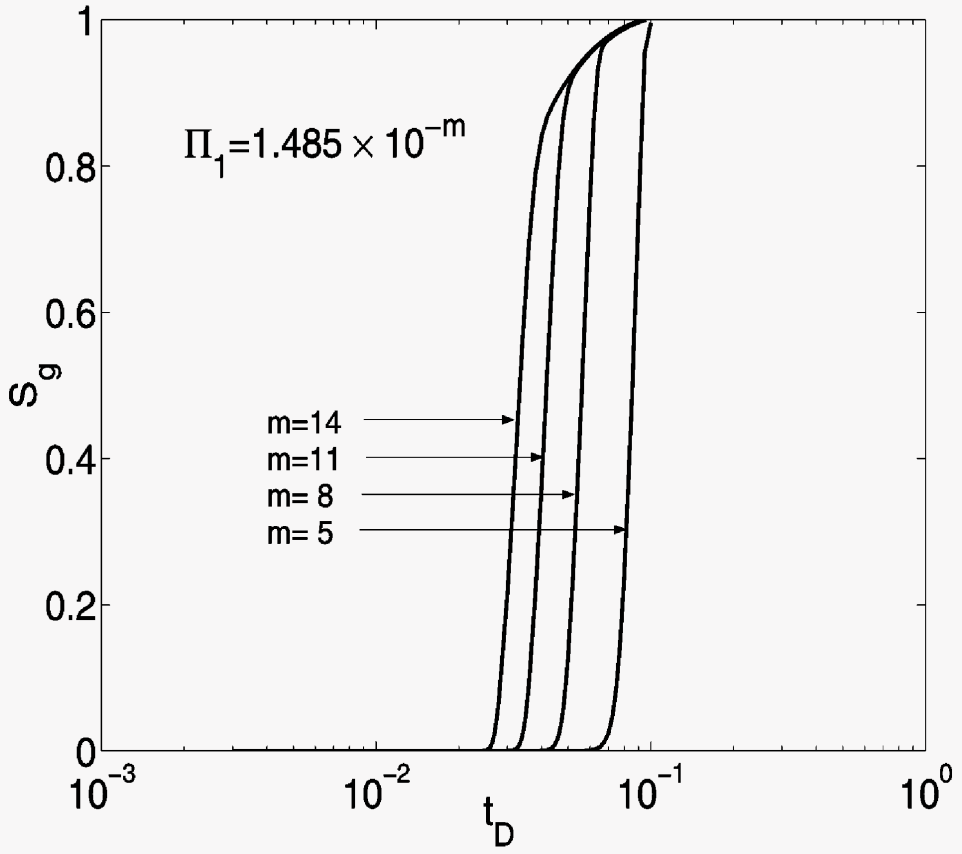

Figure 4: Variation of the gas saturation, S_g, as a function of dimensionless time, t_D. Effect of $\Pi_1 = 1.485 \times 10^{-m}$, for $\Pi_2 = 9.6972 \times 10^7$, $\Pi_\rho = 2.981$, $\Pi_c = 0.117 \times 10^1$ and $\Pi_H = 0$.

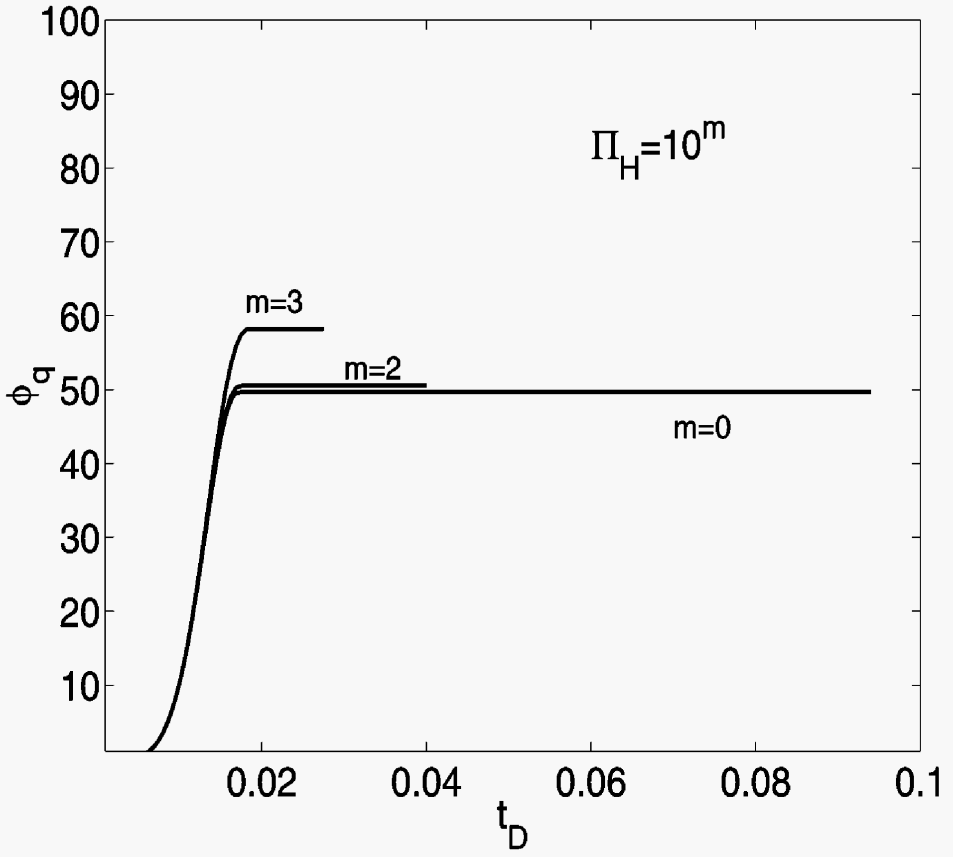

Figure 5: Variation of the rescaled nucleation fraction, ϕ_q, as a function of dimensionless time, t_D. Effect of $\Pi_H = 10^m$, for $\Pi_1 = 1.485 \times 10^{-8}$, $\Pi_2 = 9.6972 \times 10^7$, $\Pi_c = 0.117 \times 10^1$ and $\Pi_\rho = 2.981$.

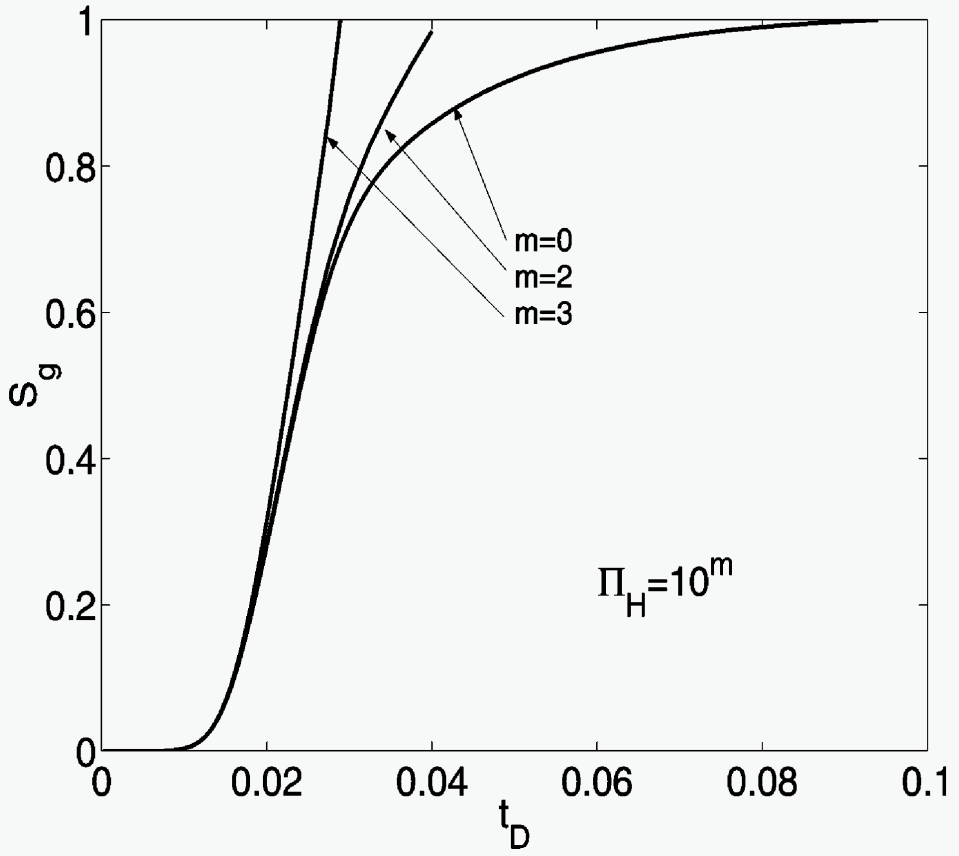

Figure 6: Variation of the gas saturation, S_g, as a function of dimensionless time, t_D. Effect of $\Pi_H = 10^m$, for $\Pi_1 = 1.485 \times 10^{-8}$, $\Pi_2 = 9.6972 \times 10^7$, $\Pi_c = 0.117 \times 10^1$ and $\Pi_\rho = 2.981$.

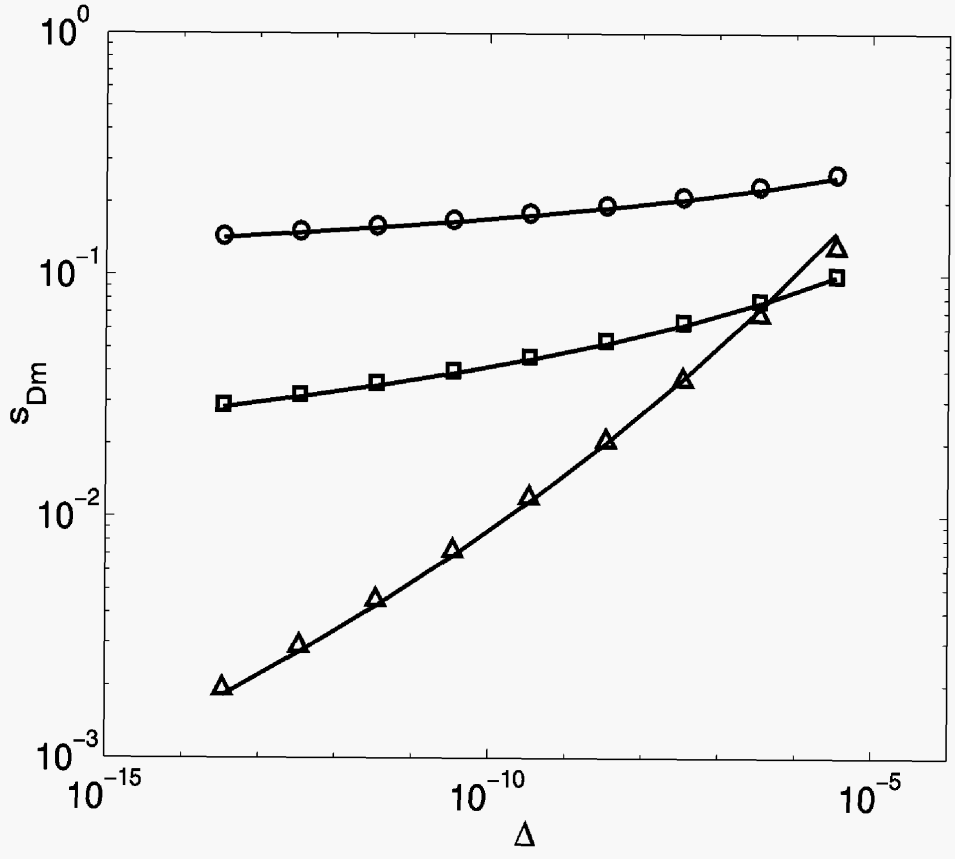

Figure 7: Maximum rescaled supersaturation, s_{Dm}, as a function of Δ for various cavity size distributions. Solid lines correspond to the simpler problem, points correspond to the full numerical solution [denoted by circles for the Rayleigh cavity size distribution, by triangles for a stretched exponential ($n = 0.2233$ and $\sigma = 0.1364$) and by squares for a stretched exponential ($n = 1.0$ and $\sigma = 1.0$)].

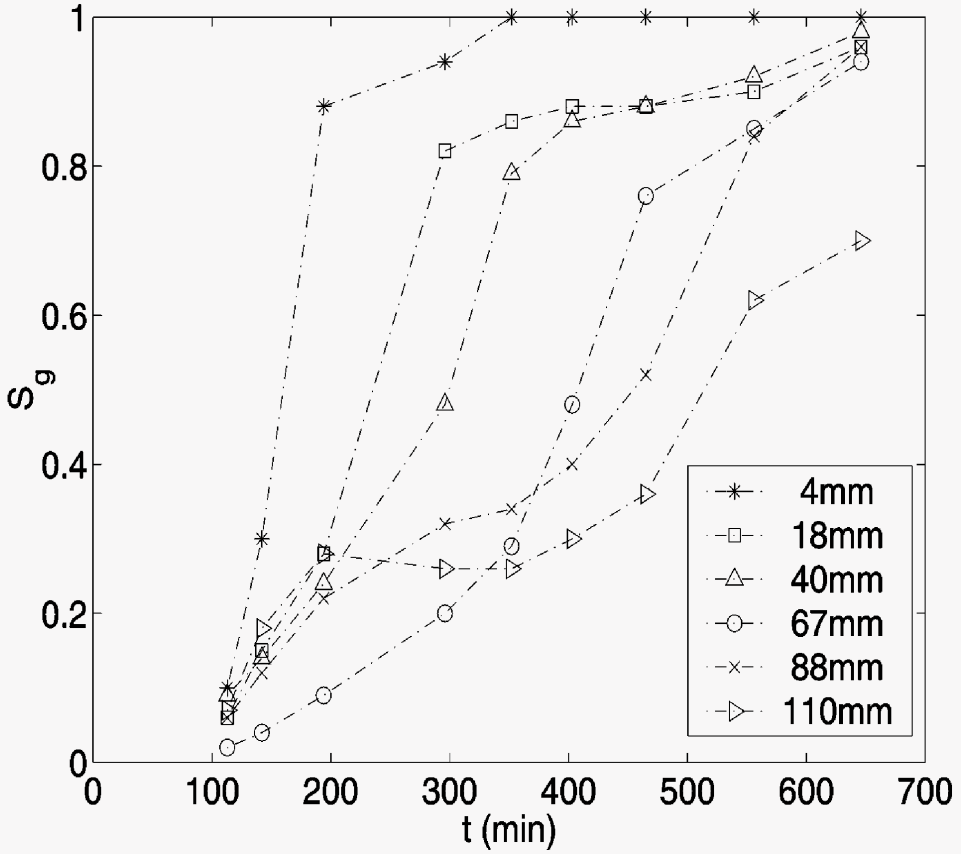

Figure 8: Gas saturation profiles for single-phase flash experiment as a function of time and for various axial positions along the core, L. Experimental data from Dehghani et al., (1997).

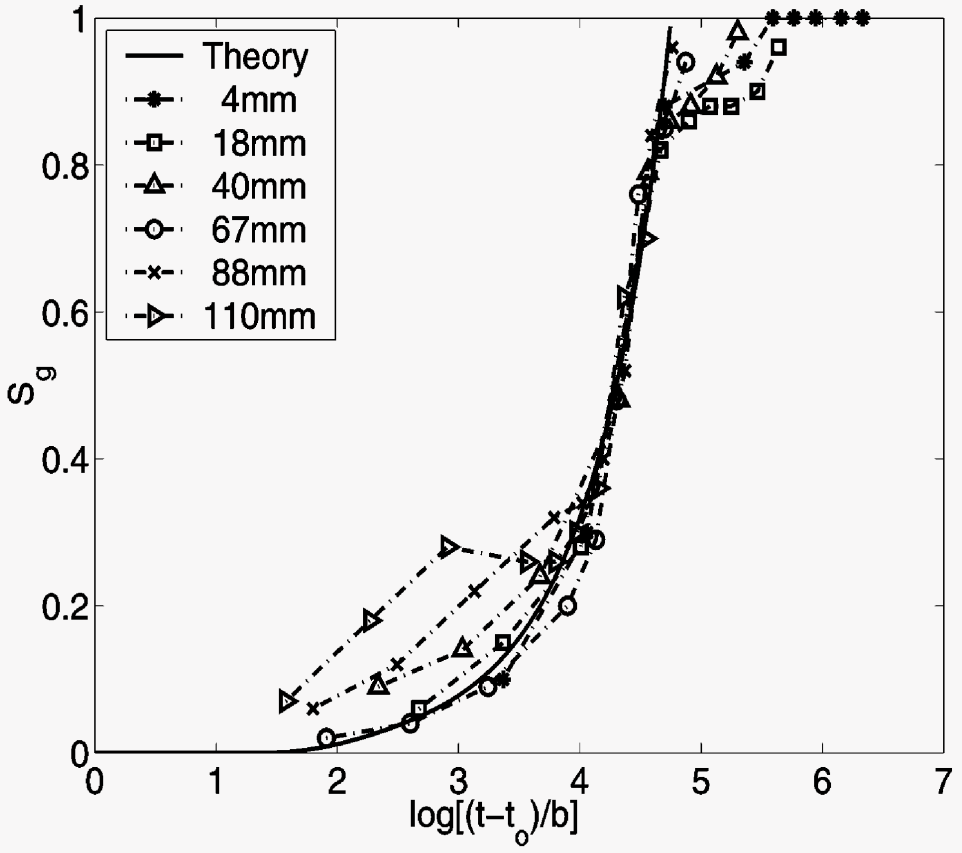

Figure 9: The evolution of the gas saturation as a function of a rescaled time for the experiments of Dehghani et al., (1997). Points denote experimental values and the solid line corresponds to the full numerical solution.

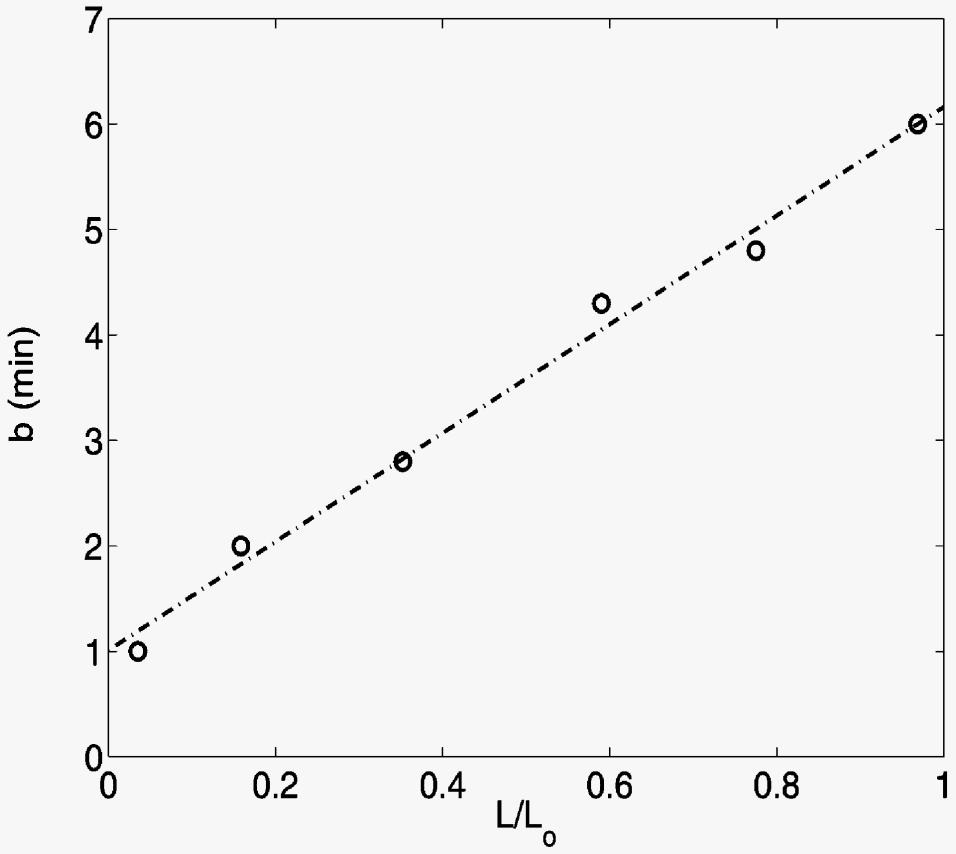

Figure 10: Variation of the rescaling factor, b, as a function of the dimensionless axial position along the core, L/L_o.